RSC Advances

PAPER

View Article Online
View Journal | View Issue

CrossMark click for updates

Cite this: *RSC Adv.*, 2016, **6**, 33811

Hierarchical mesoporous silicas templated by PE-*b*-PEO-*b*-PLA triblock copolymer for fluorescent drug delivery†

Wei-Cheng Chu,[a] Chien-Chen Cheng,[a] Bishnu Prasad Bastakoti[b] and Shiao-Wei Kuo*[ac]

Received 16th December 2015
Accepted 24th March 2016

DOI: 10.1039/c5ra26940g

www.rsc.org/advances

A series of triblock copolymers, poly(ethylene-*b*-ethylene oxide-*b*-lactide), are synthesized through ring-opening polymerization by using commercially available poly(ethylene-*b*-ethylene oxide) as a macro-initiator. Hierarchical mesoporous silica with tetragonal cylindrical and face-centered cubic pores with uniform pore size is successfully synthesized through an evaporator-induced self-assembly method using these templates. The mesoporous silica materials are characterized by small angle X-ray scattering, transmission electron microscopy and nitrogen adsorption/desorption isotherm analyses. In addition, the fluorescein isothiocyanate isomer is used as a model drug and loaded into the hierarchical mesoporous silica materials. The drug loading capacity of the materials has been measured by photoluminescence (PL) spectrophotometer at an excitation wavelength of 495 nm and emission wavelength of 518 nm, and the loading capacity is measured to be 90.4 μg mg^{-1}. It has been found that the release kinetics is influenced by the nanostructure of these hierarchical mesoporous silica materials.

Introduction

Inorganic mesoporous materials with controllable morphologies, structures, surface areas, pore sizes, pore volume, mechanical stability and biocompatibility have received much attention for their potential applications in separation, optics, adsorption, catalysis, sensors and drug delivery.[1–15] Evaporation-induced self-assembly (EISA) is a common method for the preparation of mesoporous silicas templated by amphiphilic molecules such as surfactants and block copolymers.[16–25] They are also used for the preparation of mesoporous organic materials and mesoporous carbon materials.[26–31] The triblock copolymers are also used to prepare hierarchically mesoporous materials with lamellae, and core/shell cylinders structure.[32,33] In our previous studies, ABA/BC-type block copolymer of Pluronic F127/poly(ethylene oxide-*b*-caprolactone) (PEO-*b*-PCL) as co-templates and ABC-type triblock copolymers of poly(ethylene-*b*-ethylene oxide-*b*-caprolactone) (PE-*b*-PEO-*b*-PCL) as single templates are used to prepare hierarchical mesoporous silica material through EISA. These are the first reports for the synthesis of hierarchical mesoporous silica materials by using co-templating methods of two block copolymers and single ABC-type triblock copolymers template.[34–36]

Generally the mesoporous silica materials are used as hosts for loading drugs. The drugs-loading efficiency and drugs-release kinetics are very important factors for designing the porous silica material. For example, mesoporous silica materials with the same pore size but with different mesoporous morphology (*e.g.*, hexagonal cylinder *vs.* face-centered cubic) have different drugs-loading and drugs-releasing property.[37–44] The drug loading capacity of a mesoporous silica depends on the surface area of the material while the release rate is regulated by the morphology of porous structure.[43] The most of the drugs release to surface on the both side of the hole through meso-size channel and the small part of the drugs release through the micro-size pores of inorganic wall from 2D-hexagonal cylindrical mesopore (channel-typed mesopores). In the case of 3D-face-center cubic (FCC) mesopore (cage-typed mesopores) the drugs release to surface through the micro-size pore of inorganic wall because the cage-typed mesopores only had microporous to interflow between the mesopores, in consequence, the release rate of cylindrical mesopores is faster than spherical mesopores at the same pore size. In this study (Scheme 1), we prepare the hierarchical mesoporous silica materials with tetragonal cylindrical and FCC porous structure. The mesoporous structure is confirmed by small angle X-ray scattering (SAXS), transmission electron microscope (TEM) and nitrogen adsorption and desorption isotherms. The FTIC drug is loaded into the mesoporous silica material by

[a]*Department of Materials and Optoelectronic Science, National Sun Yat-Sen University, Kaohsiung, 804, Taiwan. E-mail: kuosw@faculty.nsysu.edu.tw*

[b]*World Premier International (WPI), Research Center for Materials Nanoarchitectonics (MANA), National Institute for Materials Science (NIMS), 1-1 Namiki, Tsukuba, Ibaraki 305-0044, Japan*

[c]*Department of Medicinal and Applied Chemistry, Kaohsiung Medical University, Kaohsiung, Taiwan*

† Electronic supplementary information (ESI) available. See DOI: 10.1039/c5ra26940g

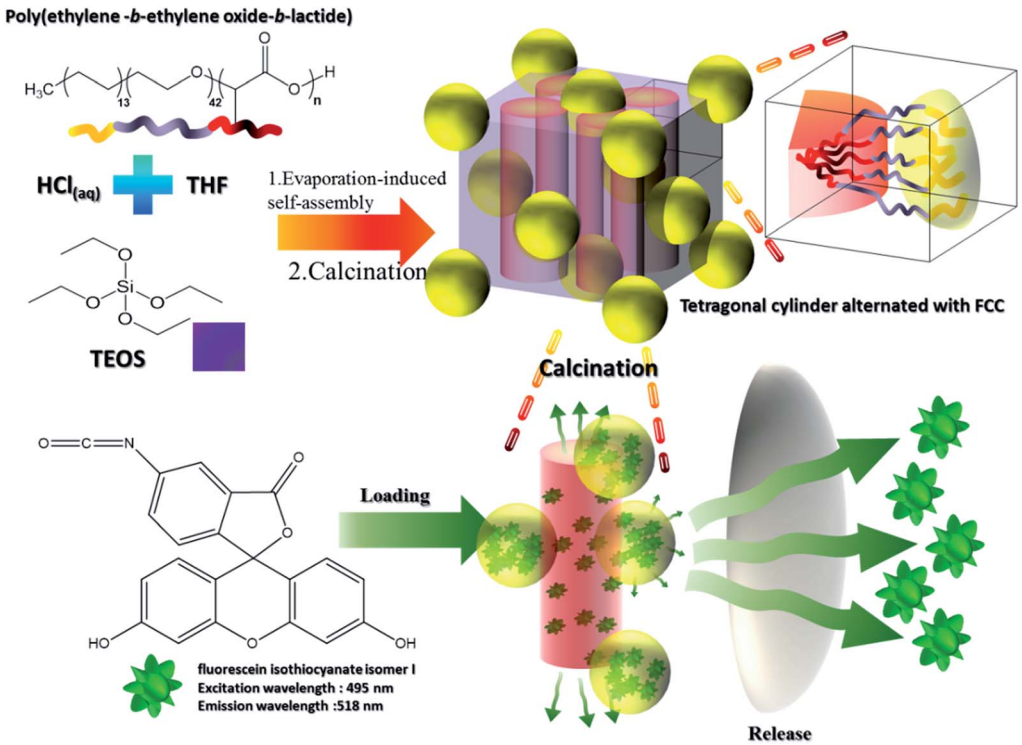

Scheme 1 Hierarchical mesoporous silicas for fluorescent drug-delivery molecule templated by PE-*b*-PEO-*b*-PLA triblock copolymer.

impregnation method and the release experiment is carried out using dialysis membrane in the phosphate buffer solution. The quantitative analysis is carried out by PL spectrophotometer at excitation wavelength of 495 nm and emission wavelength of 518 nm. The release kinetics is influenced by the hierarchical mesoporous structure of the material. The kinetic rate constant of the FITC drug molecules is determined by using power-law equation.[33]

Experimental section

Materials

PE-*b*-PEO diblock copolymer ($E_{13}EO_{42}$, M_n = 2250 g mol^{-1}, Sigma-Aldrich), 3,6-dimethyl-1,4-dioxane-2,5-dione (DL-lactide, 99%, Alfa Aesar), stannous(II) octoate ($Sn(Oct)_2$, 96%, Alfa Aesar), dichloromethane (DCM), tetrahydrofuran (THF), toluene, tetraethyl orthosilicate, hydrochloric acid (HCl, 36.5%), fluorescein isothiocyanate isomer I (FITC) and phosphate buffer solution (PBS) were purchased from Sigma-Aldrich.

Synthesis of the poly(ethylene-*block*-ethylene oxide-*block*-lactide)

The ring-opening polymerization (ROP) strategy was used to prepared the triblock copolymer of poly(ethylene-*b*-ethylene oxide-*b*-lactide) by using poly(ethylene-*b*-ethylene oxide) as marco-initiator, $Sn(Oct)_2$ as catalyst, and DL-lactide as monomer in dry toluene at 140 °C. After 12 h, the triblock copolymer was dissolved in DCM solvent and precipitated in an excess solvent of cold *n*-hexane. Finally, the sample was dried at 40 °C under vacuum. The molecular weight was determined by GPC and ^{1}H NMR (Fig. 1). Characterization of the triblock copolymers used in this study was summarized in Table 1.

Synthesis of the mesoporous silica materials

0.1 g triblock copolymer (PE-*b*-PEO-*b*-PLA), silica precursor (TEOS) and 0.10 g of 0.1 M HCl were dissolved in 5 g THF with stirring for 30 min until the solutions were homogenous. The solutions were poured into Petri dishes to evaporate the

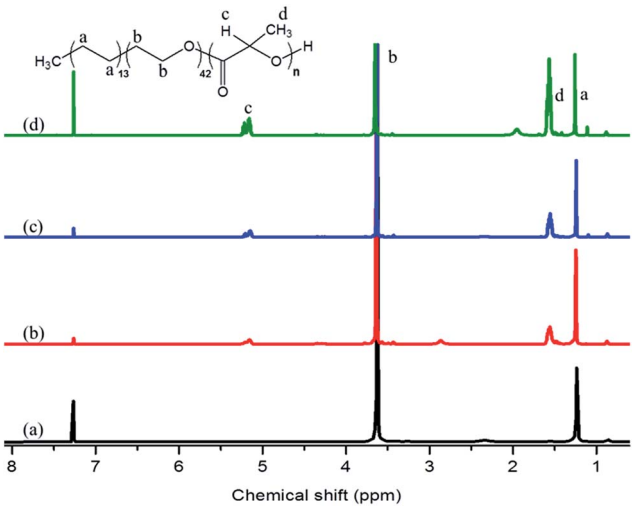

Fig. 1 ^{1}H NMR spectra of (a) PE-PEO, (b) EOA1, (c) EOA2, and (d) EOA3 in $CDCl_3$.

Table 1 The property of PE-*b*-PEO-*b*-PLA triblock copolymer used in this study

	Triblock copolymer	M_n[a]	M_n[b]	M_W[b]	M_W/M_n[b]
EOA1	E_{13}-*b*-EO_{42}-*b*-LA_{11}	3042	9800	10 600	1.08
EOA2	E_{13}-*b*-EO_{42}-*b*-LA_{26}	4122	12 200	14 000	1.14
EOA3	E_{13}-*b*-EO_{42}-*b*-LA_{61}	6642	26 900	31 800	1.18

[a] Calculate from ^{1}H NMR spectra. [b] Calculate from GPC trace with DMF eluent of 0.6 mL min^{-1} and PS-standard calibration.

solvents of THF slowly for 3 days at room temperature. The silica films were collected and grounded into powders which were poured into a PFA bottle with 10 mL of a 1.0 M HCl solution and hydrothermally heated at 100 °C for 3 days. The products were washed with water and ethanol, then dried at room temperature. Finally, the products were calcined at 500 °C for 5 h in air and collected the mesoporous silicas.

FITC load and release

1 mg of fluorescein isothiocyanate isomer I (FITC) was added into 5 mL of PBS buffer (10 mM, pH = 7.4) and stirred for 30 min, used as a primary drug solution. 10 mg of mesoporous silica material was added into the primary drug solution and stirred for 24 h. The drug loaded mesoporous silica was collected by using centrifugation with the speed of 5000 rpm and dried at 40 °C under vacuum. For the drug release experiment, 5 mg of the drug loaded mesoporous silica sample was resuspended in 5 mL of PBS buffer solution and transferred into dialysis membrane, and then immersed in 20 mL of PBS buffer solution. The experiment was carried out at 25 °C. The 2 mL of solution was taken out from the outside of dialysis membrane to check the concentration of FITC at fixed time interval under PL spectrophotometer at excitation wavelength of 495 nm and emission wavelength of 518 nm then returned it immediately.

Characterization

The gel permeation chromatography (GPC) is a Waters 510 high-performance liquid chromatograph equipped with a 410 differential refractometer which have three ultra styragel columns connected in series using dimethylformamide (DMF) as the eluent (flow rate: 0.5 mL min^{-1}) (please check it). ^{1}H NMR spectra were obtained from Varian UNITY INOVA-500 spectrometer, with the residual proton resonance of the *d*-chloroform solvent as the internal standard. Small-angle X-ray scattering from Bruker AXS, Karlsruhe, Germany with Cu Kα radiation (30 W, 50 kV, 600 μA) was used to measure the *d*-spacing. Transmission electron microscope from JEOL 3010 at 200 kV was used to observe the morphology of hierarchical mesoporous silica. TEM sample was prepared by suspending silica in ethanol and casted onto a holey carbon film of Cu grid. Nitrogen adsorption and desorption isotherms were measured using ASAP 2020 analyzer. PL spectrophotometer from Labguide X350 with 450 W Xe lamp as the light source was used to determine the concentration of FITC.

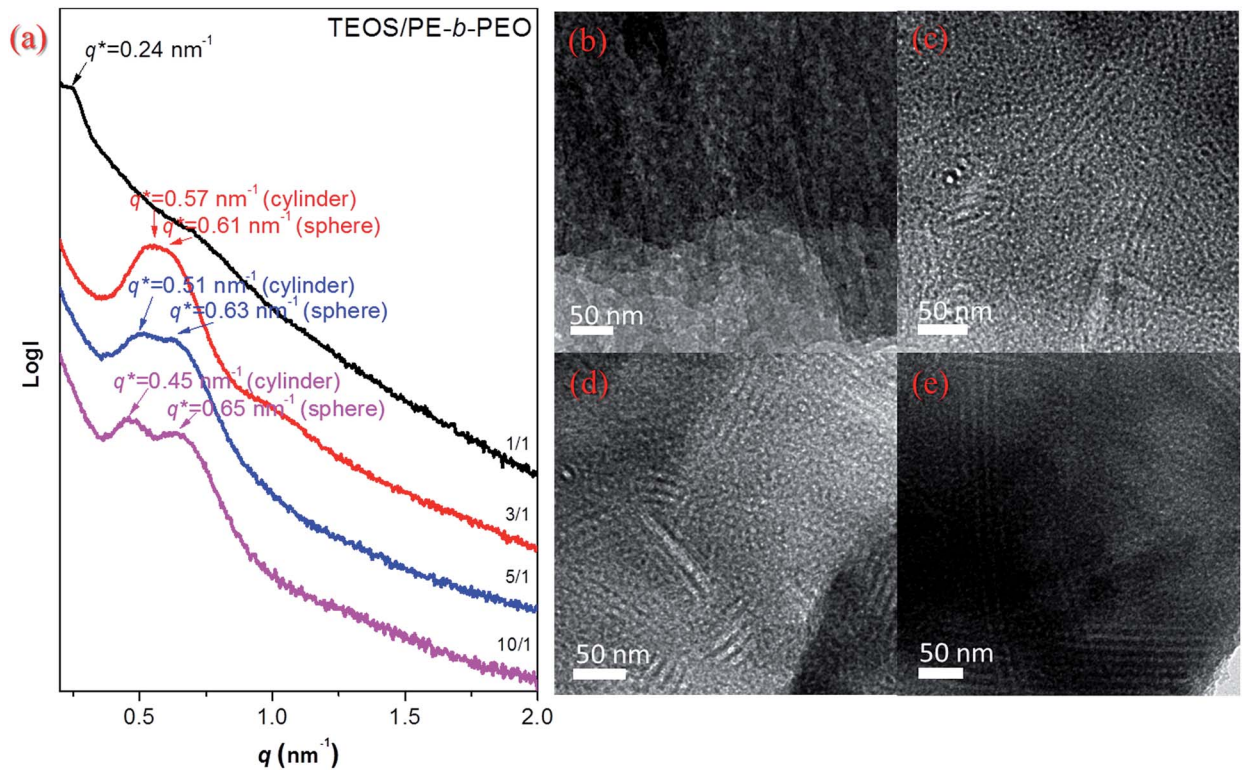

Fig. 2 (a) SAXS patterns and (b–e) TEM images of mesoporous silicas templated by PE_{13}-*b*-PEO_{42} at weight fractions of TEOS/templates = (b) 1 : 1, (c) 3 : 1, (d) 5 : 1 and (e) 10 : 1.

Results and discussion

Mesoporous silica materials templated by E_{13}-*b*-EO_{42} diblock copolymer (EOA0)

The mesoporous silica materials (Si1EOA0-to-Si10EOA0) (ex: Si*x*EOA*y*, *x* is the TEOS at *x* times weight of template and *y* is copolymer template) were prepared by employing the commercially available diblock copolymer of PE-*b*-PEO (EOA0) as template at TEOS-to-EOA0 ratios of 1 : 1, 3 : 1, 5 : 1 and 10 : 1, respectively. Fig. 2(a) and (b) show the SAXS patterns and TEM image (also Fig. S1†) of mesoporous silica of TEOS/EOA0 = 1/1, the calculated *d*-spacing is 26.1 nm with a wormhole-like structure. When the weight ratio of TEOS is increased, two different primary peaks are observed in the SAXS patterns. Similarly, a mixture of disorder cylindrical and spherical pores is clearly observed in TEM images (Fig. 2(c)–(e)). Fig. 3(a) shows the nitrogen adsorption/desorption isotherms curves at different TEOS-to-EOA0 weight ratios, indicating representative type-IV isotherms according the Brunauer, Deming, Deming, and Teller (BDDT) system. Clearly, the mesoporous silica materials at TEOS-to-EOA0 = 1/1 exhibited H_1-like hysteresis loops at values of P/P_0 ranging from 0.50 to 0.90. The mesoporous silica materials at TEOS-to-EOA0 = 3/1 exhibited two capillary condensation steps and the hysteresis loops at values of P/P_0 ranging from 0.40 to 0.80 (H_3-like loop) and 0.85 to 0.10 (H_1-like loop) which are the characteristics of spherical and cylindrical porous structure of the material.[35] Furthermore, the other two samples TEOS/EOA0 = 5/1 and 10/1 exhibits two capillary condensation steps and the hysteresis loops at values of P/P_0 ranging from 0.40 to 0.75 (H_3-like loop) and 0.75 to 1.00 (H_1-like loop). Fig. 3(b) shows the broad pore size distributions measured from the adsorption branches, based on the Barrett–Joyner–Halenda (BJH) model. The *d*-spacing, BJH pore sizes, BET surface areas, pore volumes are summarized on Table 2. The morphology of micelle changed from wormhole-like to mixture of disorder cylindrical and spherical structure with the increase of TEOS concentration.

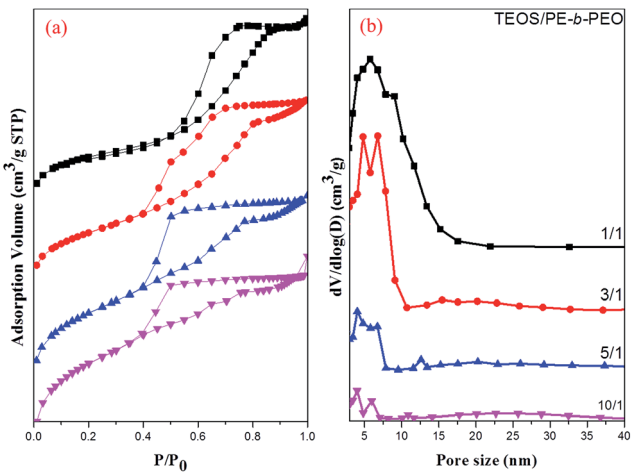

Fig. 3 (a) N_2 adsorption/desorption isotherms and (b) pore size distribution curves of mesoporous silicas templated by PE_{13}-*b*-PEO_{42} with various TEOS/PE-*b*-PEO weight ratios.

Table 2 Textural properties of mesoporous silicas templated by various block copolymers. Si*x*EOA*y*, *x* is the TEOS at *x* times weight of template and y is copolymer template

Sample (Si*x*EOA*y*)	d^a (nm)	Pore size (nm)	$S_{BET}{}^b$ ($m^2\ g^{-1}$)	Pore volume ($cm^3\ g^{-1}$)
Si1EOA0	26.1	5.9	1093.9	1.515
Si3EOA0	10.3, 11.0	4.7, 6.9	674.1	0.804
Si5EOA0	9.7, 12.3	3.9, 6.7	533.3	0.460
Si10EOA0	9.7, 14.0	4.1, 6.1	674.1	0.804
Si1EOA1	14.6	8.7	775.6	1.515
Si3EOA1	10.0	3.9, 8.4	578.0	0.680
Si5EOA1	10.3	3.3, 6.6	538.9	0.486
Si10EOA1	11.0	3.5, 7.1	399.5	0.303
Si1EOA2	16.5	12.4	688.1	1.484
Si3EOA2	14.0	5.7	591.8	0.730
Si5EOA2	10.5	5.5	437.5	0.442
Si10EOA2	10.6	7.8	237.4	0.274
Si1EOA3	17.9	17.8	1206.8	1.155
Si3EOA3	21.7	15.2	545.9	0.831
Si5EOA3	24.2	17.6	274.2	0.420
Si10EOA3	—	11.5	279.2	0.213

[a] The *d*-spacing values were calculated from the first SAXS peak by the formula $d = 2\pi/q^*$. [b] S_{BET} is the total BET surface area calculated from the *t*-plots.

Mesoporous silica materials templated by E_{13}-*b*-EO_{42}-*b*-LA_{11} (EOA1)

The PE-*b*-PEO-*b*-PLA triblock copolymer consists of two hydrophobic segments with PE and PLA, and one hydrophilic segment PEO in the center. In preview report, we choose to replace PLA by the PLLA segment, as crystalline PLLA segment preferred to from extra lamellar crystalline mesostructure and disrupt the hierarchical mesoporous structure.[30] The specific compositions of the ABC type triblock copolymers possess two different kinds of structure from PE and PLA block segment into the hierarchically microphase separation. Fig. 4(a) shows the SAXS patterns of silica materials templated by TEOS/EOA1 weight ratio 1/1, 3/1, 5/1 and 10/1 that the intensity of first peak at $q = 0.43\ nm^{-1}$ belongs to PLA segment, the others *q* about $0.60\ nm^{-1}$ belongs to PE segment. In Fig. 4(b)–(e), TEM images (also shown in Fig. S2–S4†) reveal morphology changing from wormhole-like to random spherical. Clearly, Fig. 5(a) displays the nitrogen adsorption/desorption isotherms curves at the different TEOS/EOA1 weight ratios, which represent of type-IV isotherms based on the BDDT classification system. According to the IUPAC definition, the sample of TEOS/EOA1 weight ratio 1/1 exhibit a typical H_1-like hysteresis loop at P/P_0 ranging from 0.50 to 1.00, and the others have two capillary condensation steps exhibiting H_2-like hysteresis loop at P/P_0 ranging from 0.40 to 0.65 and from 0.65 to 1.00. In addition, Fig. 5(b) displays the pore size distribution based on the BJH model. For sample; TEOS/EOA1 weight ratio 1/1 (wormhole-like pores) the material has a single peak at 8.7 nm in pore size distribution curve. The other materials have two prominent peaks in pore size distribution curve, TEOS/EOA1 = 3/1 has peaks at 3.9 and 8.4 nm, TEOS/EOA1 = 5/1 has peaks at 3.3 and

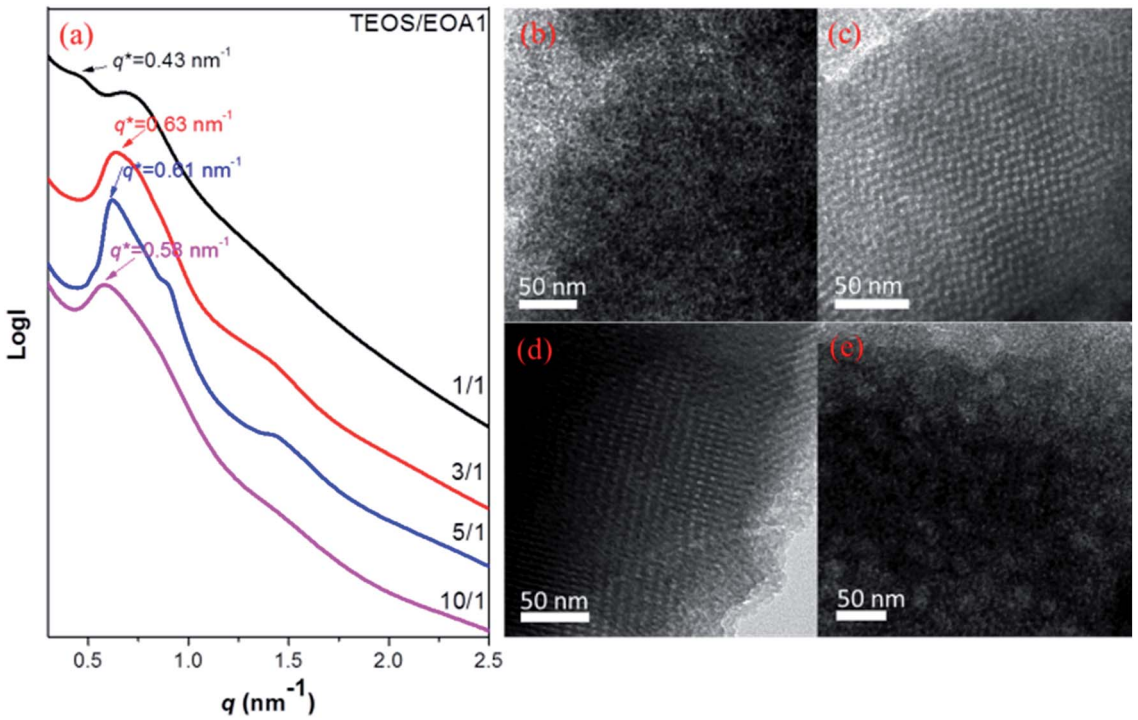

Fig. 4 (a) SAXS patterns and (b–e) TEM images of mesoporous silicas templated by PE_{13}-*b*-PEO_{42}-*b*-PLA_{11} at weight fractions of TEOS/templated = (b) 1 : 1, (c) 3 : 1, (d) 5 : 1 and (e) 10 : 1.

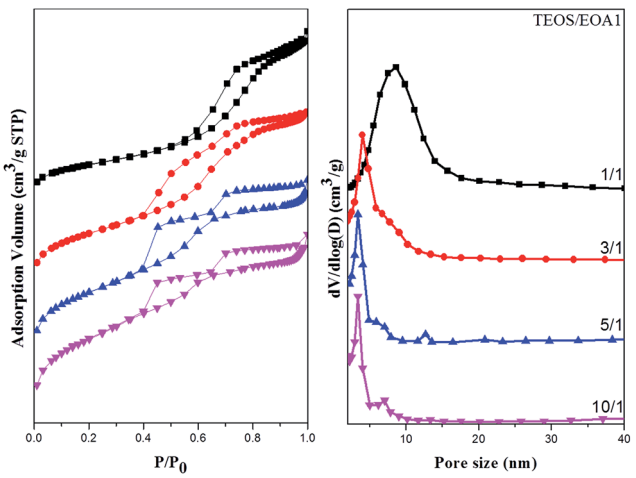

Fig. 5 (a) N_2 adsorption/desorption isotherms and (b) pore size distribution curves of mesoporous silicas templated by E_{13}-*b*-EO_{42}-*b*-LA_{11} at TEOS/templated weight fractions of 1 : 1, 3 : 1, 5 : 1, 10 : 1.

6.6 nm and TEOS/EOA1 = 10/1 has peaks at 3.5 and 7.1 nm. As a result, it was clear that the origin for bimodal pores in should come from the hydrophobic PE (smaller pore size) and PLA (larger pore size) block segments.

Mesoporous silica materials templated by E_{13}-*b*-EO_{42}-*b*-LA_{26} (EOA2)

Fig. 6 shows SAXS patterns and TEM images of mesoporous silica materials templated by EOA2. In Fig. 6(a) and (b), the SAXS patterns and TEM image of mesoporous silica TEOS/EOA2 = 1/1 with corresponding *d*-spacing of 16.5 nm, and the material has wormhole-like porous structure. Fig. 7(a) displays the N_2 adsorption/desorption isotherms curves at the different TEOS/EOA2 weight ratios, which have obviously type-IV isotherms base on the BDDT classification system. According to the IUPAC definition, in Fig. 7(a), the TEOS/EOA2 sample with weight ratio 1/1 exhibit a typical H_1-like hysteresis loop at P/P_0 ranging from 0.50 to 1.00, based on the BJH model, the pore size distributions measured a broad distribution peak at 12.4 nm as shown Fig. 7(b). In Fig. 6(a) and (c), for mesoporous silica at TEOS/EOA2 = 3/1, the SAXS pattern has broad peaks and the TEM image showed a short range order with regular spherical structure. Fig. 7(a) showed the nitrogen adsorption/desorption isotherms of the materials with TEOS/EOA2 = 3/1 and the silica material have two sharp capillary condensation steps in the relative pressure range of 0.40 to 0.75 and 0.75 to 1.00, and the results indicate the sample has two kinds of pore. The pore diameter of the material is measured to be 5.7 nm based on BJH model (Fig. 7(b)). With the increase of TEOS amount, TEOS/EOA2 = 5/1, the SAXS pattern (Fig. 6(a)) becomes sharp and the TEM image (Fig. 6(d)) shows the long range order of tetragonal cylindrical alternated with FCC structure. The detail of SAXS patterns have been shown in Fig. 8(a), the (111), (200), (220), and (311) peaks, indicating the FCC structure and the other peaks are correspond to (10), (11) and (20) peaks of the tetragonal cylindrical structure. TEM images (Fig. 8(b)–(d), also in Fig. S5†) display the [001], [100], and [110] directions that have a high degree of periodicity. This result is consistent with

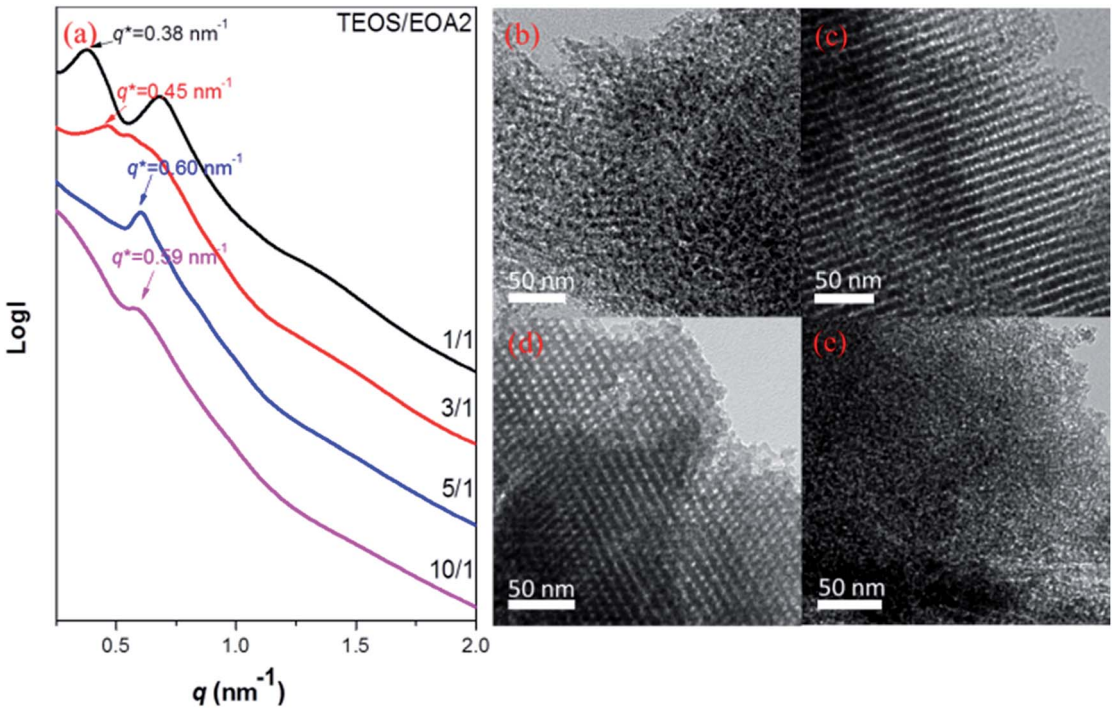

Fig. 6 (a) SAXS patterns and (b–e) TEM images of mesoporous silicas templated by E_{13}-*b*-EO_{42}-*b*-LA_{26} at weight fractions of TEOS/templated = (b) 1 : 1, (c) 3 : 1, (d) 5 : 1 and (e) 10 : 1.

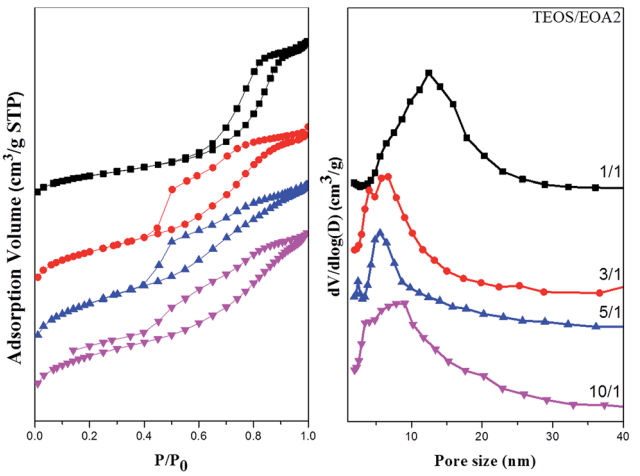

Fig. 7 (a) N_2 adsorption/desorption isotherms and (b) pore size distribution curves of mesoporous silicas templated by E_{13}-*b*-EO_{42}-*b*-LA_{26} at TEOS/templated weight fractions of 1 : 1, 3 : 1, 5 : 1, 10 : 1.

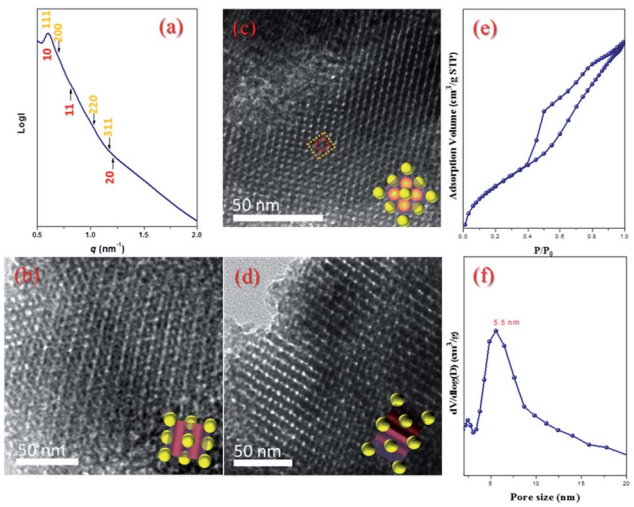

Fig. 8 (a) SAXS pattern and TEM images viewed from the (b) [001], (c) [100], (d) [110] directions. (e) N_2 adsorption/desorption isotherms and (f) pore size distribution curves of mesoporous silicas templated by E_{13}-*b*-EO_{42}-*b*-LA_{26} at weight fractions of TEOS/PE-*b*-PEO-PLA = 5/1.

our previous study.[34–36] Fig. 8(b) displays two kinds of mesopores and staggered tetragonal packing along [001] direction, because the FCC structure are square arrangement along [001] direction and the tetragonal cylinder also are square arrangement along [001] direction. In addition, the FCC structure also are square arrangement along [100] direction and the tetragonal cylinder are parallel columnar arrangement, so Fig. 8(c) shows the sphere of FCC included into the walls of cylinder of tetragonal cylinder along [100] direction. Along [110] direction, the FCC structure are hexagonal close-packed along [110] direction and the tetragonal cylinder also are parallel columnar arrangement. Consequently, TEM image (Fig. 8(d)) shows the sphere of FCC was stacked around the helix-like wall. TEM images show that the texture of the mesoporous silica contains two different structures of pores with same pore size (*ca.* 5.5 nm). The mesoporous of FCC are prepared by the PE segment, and the mesoporous of tetragonal cylinder are prepared by the PLA segment. Fig. 8(e) shows the nitrogen adsorption/

desorption isotherms of mesoporous silica material and according to IUPAC definition, the material with tetragonal cylinder alternated with FCC will have type-IV isotherm.[35] According the BDDT classification system, the results indicate the hierarchical mesoporous silicas with two kinds of pore size, and the sample exhibit two hysteresis loops at $P/P_0 = 0.40$ to 0.75 with H_2-like loop and $P/P_0 = 0.75$ to 1.00 with H_1-like loop which clearly indicate the presence of two types of mesopores; spherical and cylindrical respectively. In Fig. 8(f), based on the BJH model, the pore size distribution curve has been shown and from the adsorption branch the pore diameter is measured to be 5.5 nm. Further with increasing the TEOS amount in TEOS–EOA2 mixture, when the TEOS/EOA2 = 10/1, the corresponding SAXS patterns and TEM images are shown in Fig. 6(a) and (e). The corresponding *d*-spacing is measured to be 10.6 nm with wormhole-like porous structure. In Fig. 7(a), the sample of TEOS/EOA2 = 10/1 exhibits a typical H_1-like hysteresis loop at P/P_0 ranging from 0.40 to 1.00, based on the BJH model, the pore size distributions measured to be 7.8 nm as shown in Fig. 7(b).

Mesoporous silica materials templated by E_{13}-*b*-EO_{42}-*b*-LA_{61} (EOA3)

The mesoporous silica samples are discussed here is templated by E_{13}-*b*-EO_{42}-*b*-LA_{61} (EOA3) at TEOS/EOA3 ratios of 1 : 1, 3 : 1, 5 : 1 and 10 : 1, respectively. Fig. 9 displays the SAXS patterns of the materials and the corresponding *d*-spacings of the mesoporous silica materials are increased from 17.9 nm, 21.7 nm, 24.2 nm with increasing the TEOS amount in the mixture. In agreement, Fig. 9(b)–(e) of the TEM images revealed that morphology are wormhole-like mesoporous structure and the pore size increased with increasing the TEOS amount. According to the BDDT classification system, in Fig. 10(a), all the mesoporous silica materials provided typical type-IV isotherms in nitrogen adsorption/desorption isotherms. The TEOS : EOA3 ratios of 1 : 1 and 3 : 1 exhibited H_1-like hysteresis loops (slit-like) at values of P/P_0 ranging from 0.40 to 1.00 and the TEOS/EOA3 ratios of 5 : 1 and 10 : 1 exhibited H_3-like hysteresis loops at values of P/P_0 ranging from 0.40 to 1.00. In Fig. 10(b), based on the BJH model, the pore size distributions show pore diameter of 17.8 nm, 15.2 nm, 17.6 nm and 11.5 with the TEOS

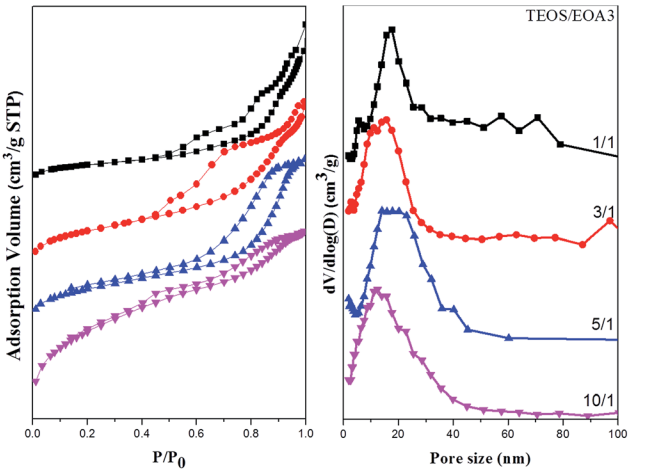

Fig. 10 (a) N_2 adsorption/desorption isotherms and (b) pore size distribution curves of mesoporous silicas templated by E_{13}-*b*-EO_{42}-*b*-LA_{61} at TEOS/templated weight fractions of 1 : 1, 3 : 1, 5 : 1, 10 : 1.

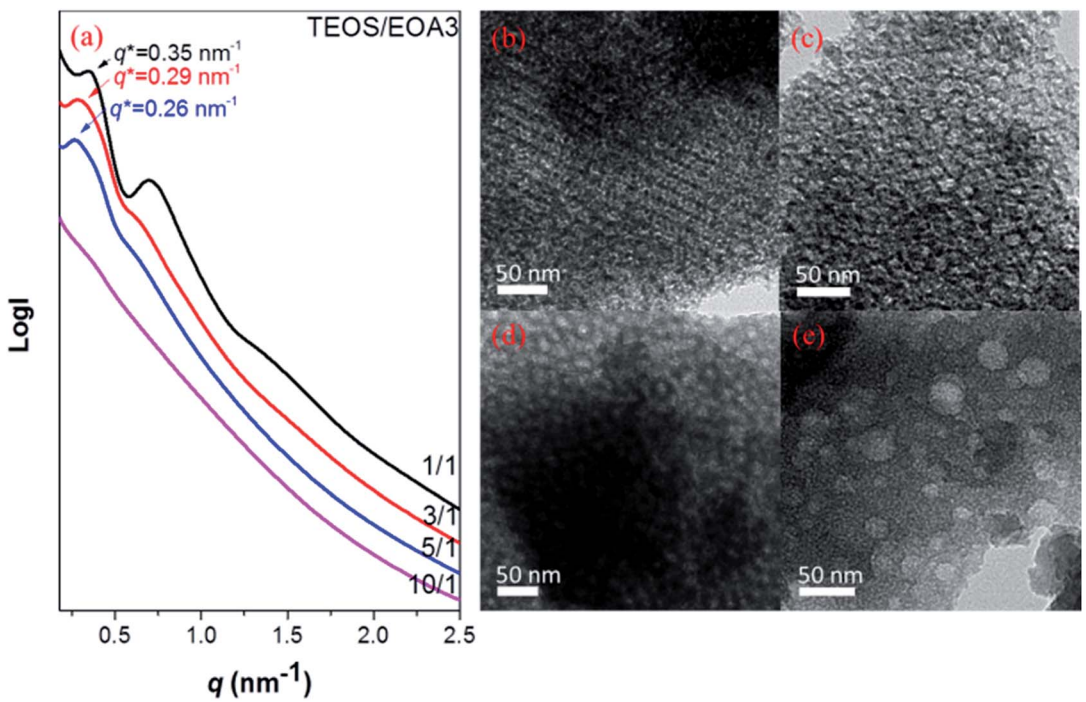

Fig. 9 (a) SAXS patterns and (b–e) TEM images of mesoporous silicas templated by E_{13}-*b*-EO_{42}-*b*-LA_{61} at weight fractions of TEOS/templated = (b) 1 : 1, (c) 3 : 1, (d) 5 : 1 and (e) 10 : 1.

weight increasing. Table 2 summarizes the *d*-spacing, BJH pore size distributions, the BET surface areas and pore volumes of these mesoporous silica materials. Clearly, the pore size was generally decreased with the increase of TEOS concentration at lower than TEOS/templates = 5/1. Further increase the TEOS concentration to TEOS/templates = 10/1, the random trend was observed since the disorder structures were observed in these compositions. In addition, we maintain the TEOS/templates = 5/1 ratio to understand the effect of molecular weights of PLA in triblock copolymers on the porous structures as following section.

Mesoporous silica materials at TEOS/Template weight ratios of 5 : 1

TEOS/template = 5/1 are the more order morphology of mesoporous silica. The SAXS patterns, TEM images, nitrogen adsorption/desorption isotherms and pore size distributions of the mesoporous silica materials prepared by using TEOS/template = 5/1 have been shown in Fig. 11. Fig. 11(a) shows the SAXS patterns of silica materials templated by TEOS/EOA1 that the peak position at 0.60 nm^{-1} belongs to PE segment. We observe that upon increasing the molecular weight of the PLA segments, the *d*-spacing was increased. Clearly, the TEM images (Fig. 11(b)–(d)) revealed that the morphology transformed from a short range order spherical structure to tetragonal cylindrical alternated with FCC and, finally, to a disordered micelle structure and the *d*-spacing increased upon increasing the molecular weight of the PLA segments. In Fig. 11(e), the N_2 sorption isotherms of mesoporous silica samples are all type-IV curves; all the samples provide clear isotherms curves with two capillary condensation steps exhibiting H_2-like and H_3-like hysteresis loops. Fig. 11(f) displays the pore size distributions, measured from the adsorption branches, upon increasing the molecular weight of the PLA segments, the average pore size increased.

Release of FITC molecules into hierarchical mesoporous silica material

In Scheme 1, we have represented the evaporator-induced self-assembly method to prepared hierarchical mesoporous silica material with single triblock copolymer template PE-*b*-PEO-*b*-PLA at various weight ratios. The morphology of hierarchical mesoporous silica material Si5EOA2 is examined to be cylindrical alternated with FCC. This is a particular structure which have both sphered and cylinder mesoporous structure; the sphere mesoporous of FCC are prepared by the PE segment and the cylinder mesoporous of tetragonal cylinder are prepared by

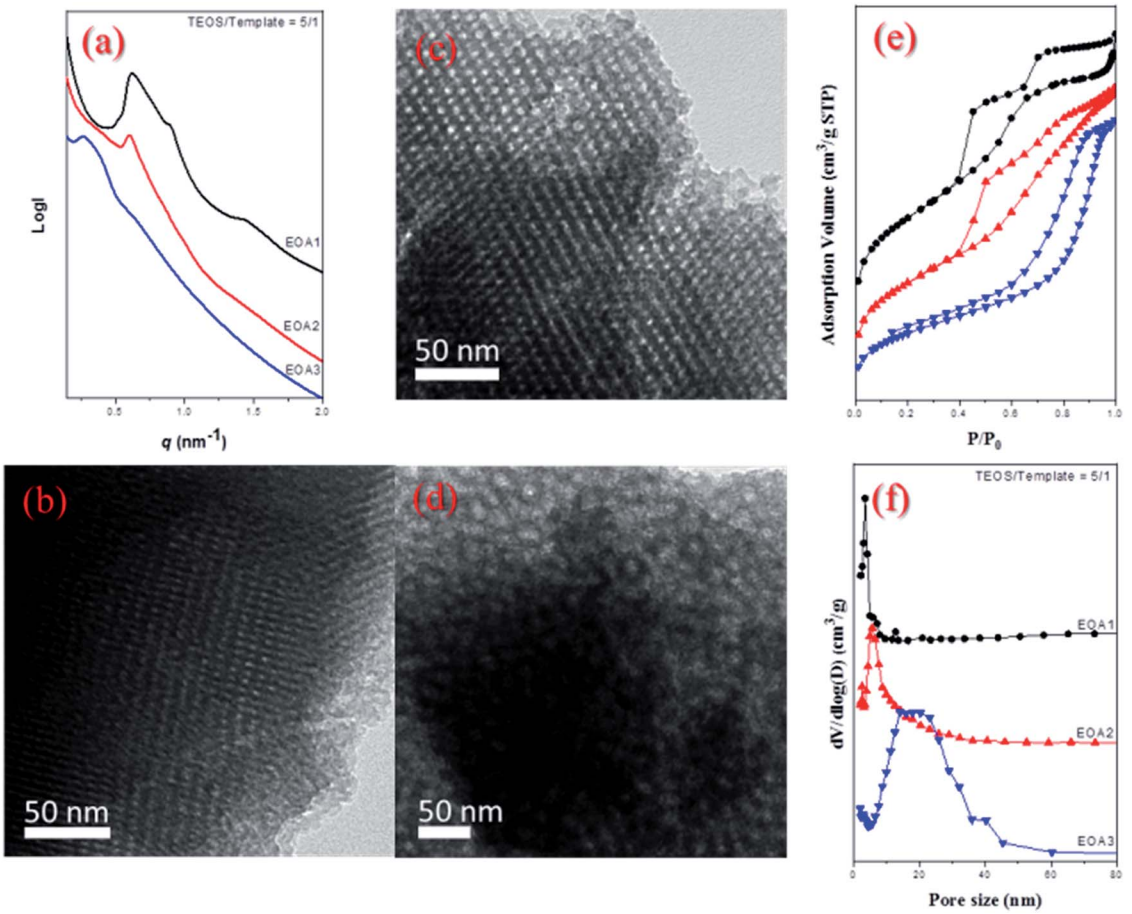

Fig. 11 (a) SAXS patterns and (b–e) TEM images of mesoporous silicas templated by = (b) EOA1, (c) EOA2 (d) EOA3, (e) N_2 adsorption/desorption isotherms and (f) pore size distribution curves of mesoporous silicas at TEOS/templated weight fractions of 5 : 1.

the PLA segment. The Si5EOA1 is random sphere structure with two pore distributions of 3.3 and 6.6 nm. In Fig. 12, cumulative release *vs.* time plot demonstrates a steady drugs-release in the 30 hours which then saturates as measured by PL spectrophotometer. In order to quantify the release parameter we fit our data to Peppas equation; $M_t/M_\infty = kt^n$ where M_t is the amount of FITC release at time t, M_∞ is the total amount of drug-release at infinite time, k is the release constant, and the n is the exponent of the drugs-release mechanism. A diffusion exponent $n = 1$ means that the drug release is independent of time, regardless of the geometry and it indicate zero order release. If $n = 0.5$, it indicates swelling diffusion mechanism (Fickian diffusion). If n is 0.5 to 1.0, it indicates anomalous (non-Fickian) transport (effects by swelling and stresses). In this case, the n equal to 0.61 (Si5EOA1) and 0.90 (Si5EOA2) and mechanism is non-Fickian transport. Characterization of drug delivery experiment was summarized in Table 3. In the Fig. 12, the hierarchical mesoporous silica material Si5EOA2 can release 83.7% FITC and the random sphere mesoporous silica material Si5EOA1 only can release 32.5% within 2 h. In addition, we also compare with the typical mesoporous silica (SBA-15), it only release *ca.* 13% within 2 h of FITC-based compound.[45] In the saturation, the Si5EOA2 is 100%, Si5EOA1 is 40%, and SBA-15 is *ca.* 20% drug release. Because of only cylinder structure of SBA-15, the cumulative and time release is smaller than Si5EOA2 and Si5EOA1. In addition, Fig. 13 shows the cumulative release amount, the loading capacity of Si5EOA2 is as high as up to 90.4

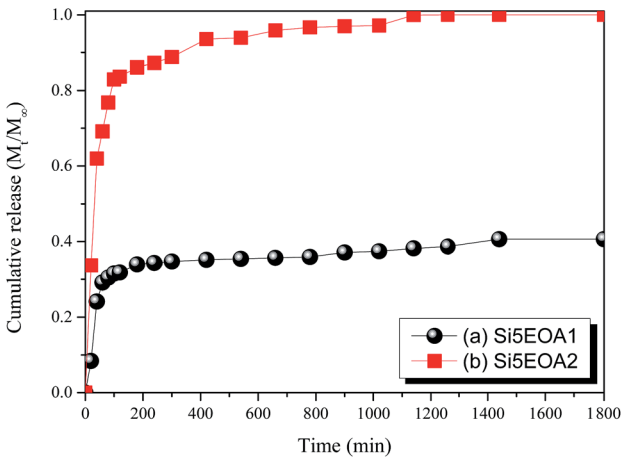

Fig. 12 Cumulative release profiles of FITC with hierarchical mesoporous silica material of (a) Si5EOA1 and (b) Si5EOA2.

Table 3 Textural properties of drug delivery experiment

Sample	K (constant)[a]	n (diffusion exponent)[a]	Loading capacity[b] (μg mg^{-1})
Si5EOA1	60	0.61	23.8
Si5EOA2	112	0.90	90.4

[a] The n & k values were calculated from the simple linear regression for the power law equation. [b] Loading capacity are calculated from the calibration curve within 30 hours.

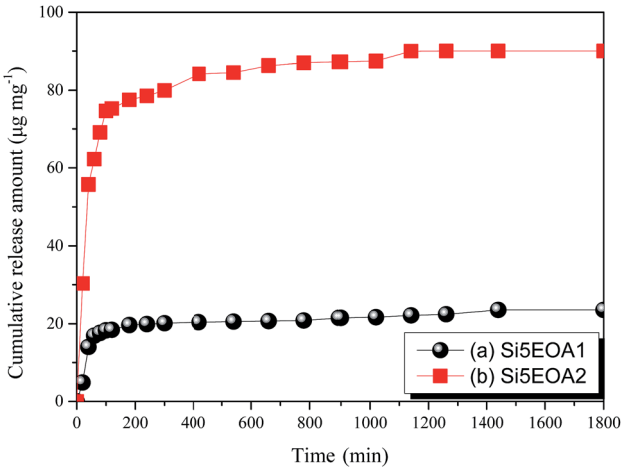

Fig. 13 Release amount of FITC with hierarchical mesoporous silica material of (a) Si5EOA1 and (b) Si5EOA2.

μg mg^{-1} and the other is 23.8 μg mg^{-1}, because the physical absorption and desorption forces are different for spherical and cylindrical porous. In the preview report, the spherical and cylindrical porous has different release rate.[40] The physical desorption rate for spherical FCC is slower then tetragonal cylindrical. A partial of FTIC is remained in random sphere mesoporous silica material Si5EOA1; because the drug delivery is difficult through micro channels between spheres and the FTIC have hydrogen bonding interaction with the surface of mesoporous silica. The release of hierarchical mesoporous silica material Si5EOA2 have the both spherical and cylindrical porous that have the better release condition compared with Si5EOA1 and SBA-15. As a result, the release rate is influenced with the hierarchical mesoporous silica material.

Conclusions

The hierarchical mesoporous silica material of tetragonal cylinder alternated with FCC with uniform pore size is successfully synthesized through evaporation-induced self-assembly method. The physical absorption and desorption forces are different for nanostructure including spherical and cylindrical porous. The hierarchical mesoporous silica material is loaded by FTIC and release is studied using dialysis method in the phosphate buffer solution. The amount of loaded/delivered drug is measured by PL spectrophotometer. The kinetics and mechanisms of FITC release are determined by using power-law equation that the value n equal to n equal to 0.61 (Si5EOA1) and 0.90 (Si5EOA2) and mechanism is non-Fickian transport. The loading capacity of Si5EOA2 is high up to 90.4 μg mg^{-1} and the release kinetic is influenced by nanostructure of the hierarchical mesoporous silica material.

Acknowledgements

This study was financially supported by the Ministry of Science and Technology, Taiwan, under contracts MOST 103-2221-E-

110-079-MY3. Prof. Shiao-Wei Kuo also would like to thank 2014 New Partnership Program for the Connection to the Top Labs in the World, also supported by the Ministry of Science and Technology, Taiwan, under contracts MOST 103-2911-I-110-513 that helped initiate this study.

References

1 X. Zhuang, Y. Wan, C. M. Feng, Y. Shen and D. Y. Zhao, *Chem. Mater.*, 2009, **21**, 706.
2 K. Nakajima, T. Fukui, H. Kato, M. Kitano, J. N. Kondo, S. Hayashi and M. Hara, *Chem. Mater.*, 2010, **22**, 3332.
3 H. A. Meng, M. Liong, T. A. Xia, Z. X. Li, Z. X. Ji, J. I. Zink and A. E. Nel, *ACS Nano*, 2010, **4**, 4539.
4 N. Hao, Y. X. Yang, H. T. Wang, P. A. Webley and D. Y. Zhao, *J. Colloid Interface Sci.*, 2010, **346**, 429.
5 B. P. Bastakoti, N. L. Torad and Y. Yamauchi, *ACS Appl. Mater. Interfaces*, 2014, **6**, 854.
6 H. Yamada, C. Urata, S. Higashitamori, Y. Aoyama, Y. Yamauchi and K. Kuroda, *ACS Appl. Mater. Interfaces*, 2014, **6**, 3491.
7 Y. Zhang, C. Y. Ang, M. Li, S. Y. Tan, Q. Qu, Z. Luo and Y. Zhao, *ACS Appl. Mater. Interfaces*, 2015, **7**, 18179.
8 T. L. Chew, A. L. Ahmad and S. Bhatia, *Adv. Colloid Interface Sci.*, 2010, **153**, 43.
9 Q. Gao, W. J. Xu, Y. Xu, D. Wu, Y. H. Sun, F. Deng and W. L. Shen, *J. Phys. Chem. B*, 2008, **112**, 2261.
10 Q. J. He and J. L. Shi, *J. Mater. Chem.*, 2011, **21**, 5845.
11 B. V. Lotsch and G. A. Ozin, *ACS Nano*, 2008, **2**, 2065.
12 H. A. Meng, M. Liong, T. A. Xia, Z. X. Li, Z. X. Ji, J. I. Zink and A. E. Nel, *ACS Nano*, 2010, **4**, 4539.
13 J. G. Li, T. S. Lee, K. U. Jeong, C. H. Lin and S. W. Kuo, *RSC Adv.*, 2012, **2**, 11242.
14 M. Vallet-Regi, F. Balas and D. Arcos, *Angew. Chem., Int. Ed.*, 2007, **46**, 7548.
15 S. Angelos, M. Liong, E. Choi and J. I. Zink, *Chem. Eng. J.*, 2008, **137**, 4.
16 J. Y. Zhang, Y. H. Deng, J. Wei, Z. K. Sun, D. Gu, H. Bongard, C. Liu, H. H. Wu, B. Tu, F. Schuth and D. Y. Zhao, *Chem. Mater.*, 2009, **21**, 3996.
17 Y. H. Deng, J. Liu, C. Liu, D. Gu, Z. K. Sun, J. Wei, J. Y. Zhang, L. J. Zhang, B. Tu and D. Y. Zhao, *Chem. Mater.*, 2008, **20**, 7281.
18 Y. Deng, C. Liu, D. Gu, T. Yu, B. Tu and D. Zhao, *J. Mater. Chem.*, 2008, **18**, 91.
19 O. Altukhov and S. W. Kuo, *RSC Adv.*, 2015, **5**, 22625.
20 Y. Huang, J. P. Yang, H. Q. Cai, Y. P. Zhai, D. Feng, Y. H. Deng, B. Tu and D. Y. Zhao, *J. Mater. Chem.*, 2009, **19**, 6536.
21 E. Nisson, Y. Sakamoto and A. E. C. Palmqvist, *Chem. Mater.*, 2011, **23**, 2781.
22 J. G. Li, W. C. Chen and S. W. Kuo, *Microporous Mesoporous Mater.*, 2012, **163**, 34.
23 D. Grosso, C. Boissiere, B. Smarsly, T. Brezesinski, N. Pinna, P. A. Albouy, H. Amenitsch, M. Antonietti and C. Sanchez, *Nat. Mater.*, 2004, **3**, 787.
24 E. Ortel, A. Fischer, L. Chuenchom, J. Polte, F. Emmerling, B. Smarsly and R. Kraehnert, *Small*, 2012, **8**, 298.
25 K. Kailasam, Y. S. Jun, P. Katekomol, J. D. Epping, W. H. Hong and A. Thomas, *Chem. Mater.*, 2010, **22**, 428.
26 W. C. Chu, S. F. Chiang, J. G. Li and S. W. Kuo, *RSC Adv.*, 2014, **4**, 784.
27 W. C. Chu, C. X. Lin and S. W. Kuo, *RSC Adv.*, 2014, **4**, 61012.
28 H. J. Lee, R. L. Jones, D. Y. Zhao and B. D. Vogt, *J. Mater. Chem.*, 2010, **20**, 1691.
29 C. Urata, Y. Tamura, Y. Yamauchi and K. Kuroda, *J. Mater. Chem.*, 2011, **21**, 3711.
30 J. G. Li, W. C. Chu, C. W. Tu and S. W. Kuo, *J. Nanosci. Nanotechnol.*, 2013, **13**, 2495.
31 M. Suh, H. J. Lee, J. Y. Park, U. H. Lee, Y. U. Kwon and D. Kim, *ChemPhysChem*, 2008, **9**, 1402.
32 H. Y. Lian, Y. H. Liang, Y. Yamauchi and K. C.-W. Wu, *J. Phys. Chem. C*, 2011, **115**, 6581–6590.
33 J. Siepmann and N. A. Peppas, *Adv. Drug Delivery Rev.*, 2001, **48**, 139.
34 J. G. Li, R. B. Lin and S. W. Kuo, *Macromol. Rapid Commun.*, 2012, **33**, 678.
35 J. G. Li, R. B. Lin and S. W. Kuo, *RSC Adv.*, 2013, **3**, 17411.
36 C. C. Liu, J. G. Li and S. W. Kuo, *RSC Adv.*, 2014, **4**, 20262.
37 B. P. Bastakoti, S. H. Liao, M. Inoue, S. I. Yusa, M. Imura, K. Nakashima, K. C. W. Wu and Y. Yamauchi, *Sci. Technol. Adv. Mater.*, 2013, **14**, 044402.
38 B. P. B. Bastakoti, K. C. W. Wu, M. Inoue, S. I. Yusa, K. Nakashima and Y. Yamauchi, *Chem.–Eur. J.*, 2013, **19**, 4812.
39 C. Urata, Y. Tamura, Y. Yamauchi and K. Kuroda, *J. Mater. Chem.*, 2011, **21**, 3711.
40 H. Y. Lian, Y. H. Liang, Y. Yamauchi and K. C.-W. Wu, *J. Phys. Chem. C*, 2011, **115**, 6581.
41 M. Vallet-Regi, F. Balas and D. Arcos, *Angew. Chem., Int. Ed.*, 2007, **46**, 7548.
42 C. W. Wu, Y. Yamauchi, T. Ohsuna and K. Kuroda, *J. Mater. Chem.*, 2006, **16**, 3091.
43 N. Chen, S. Cheng, J. S. Souris, C. Chen, C. Mou and L. Lo, *J. Mater. Chem. B*, 2013, **1**, 3128.
44 M. Ferenc, N. Katir, K. Milowska, M. Bousmina, J. Majoral, M. Bryszewska and A. El Kadib, *J. Mater. Chem. B*, 2015, **3**, 2714.
45 T. W. Kim, I. I. Slowing, P. W. Chung and V. S. Y. Lin, *ACS Nano*, 2011, **5**, 360.

